Supporting Information for

Metastable phase platinum oxide clarifying Pt-O active site for hydrogen evolution reaction

Haiwei Yang, [#1] Yujin Ji, [#1] Qi Shao, *[2] Wenxiang Zhu, [1] Miaomiao Fang, [2] Mengjie Ma, [1] Fan Liao, [1] Hui Huang, [1] Yi Zhang, [1] Junjun Yang, [1] Zhenglong Fan, [1] Youyong Li, [1] Yang Liu, *[1] Mingwang Shao, *[1] and Zhenhui Kang, *[1,3]

[1]Institute of Functional Nano & Soft Materials (FUNSOM), Soochow University, Jiangsu 215123, China.

[2]College of Chemistry, Chemical Engineering and Materials Science, Soochow University, Jiangsu 215123, China.

[3] Macao Institute of Materials Science and Engineering (MIMSE), MUST−SUDA Joint Research Center for Advanced Functional Materials, Macau University of Science and Technology, Taipa 999078, Macao, China.

*Correspondence to: qshao@suda.edu.cn; yangl@suda.edu.cn; mwshao@suda.edu.cn; zhkang@suda.edu.cn

[#]These authors are contributed equally.

Supporting Figures

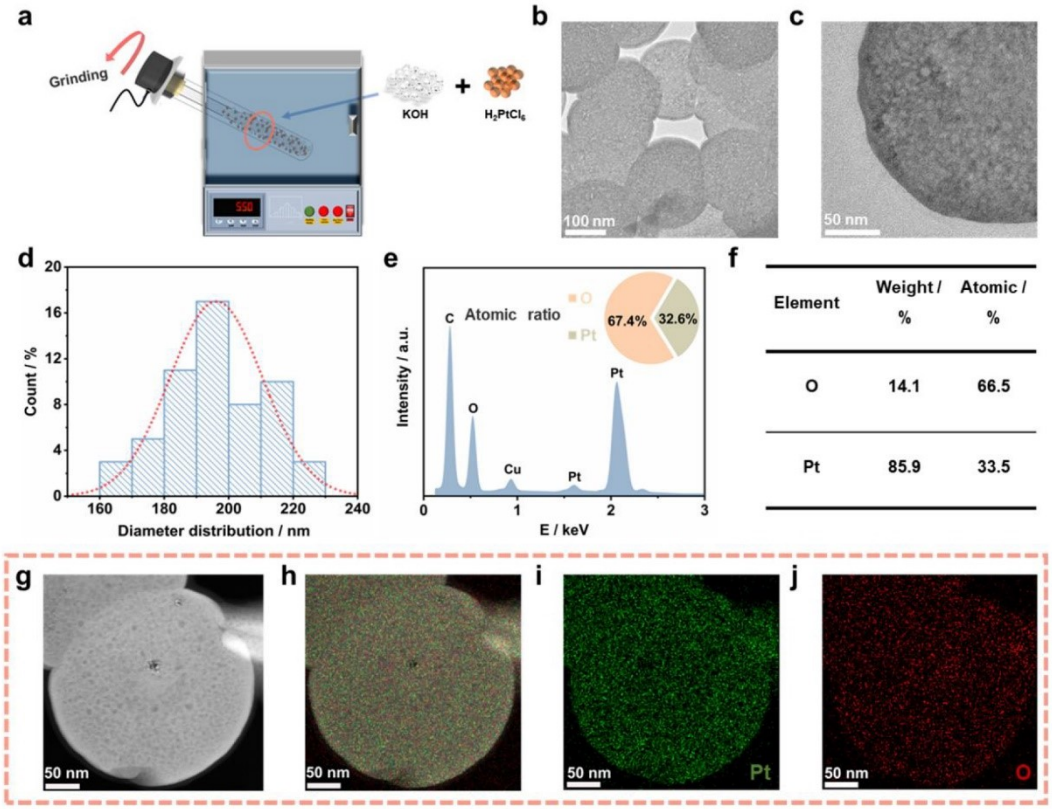

Figure S1. Structural characterizations of 1T-PtO_2. (**a**) Schematic illustration of the fabrication of 1T-PtO_2 via the molten alkali mechanochemical method. (**b**, **c**) Transmission electron microscopy (TEM) images of 1T-PtO_2, showing the nanosheets morphology. (**d**) Diameter distribution of 1T-PtO_2 nanosheets obtained by SEM and TEM (the average diameter is 200 nm). (**e**) TEM energy-dispersive X-ray spectroscopy (TEM-EDX) result. The atomic ratio of Pt and O is about 1 : 2. (**f**) Summary table of weight ratio and atomic ratio of Pt and O obtained from elemental analysis. (**g-j**) STEM-EDX mapping of 1T-PtO_2, where Pt (green) and O (red) are uniformly distributed.

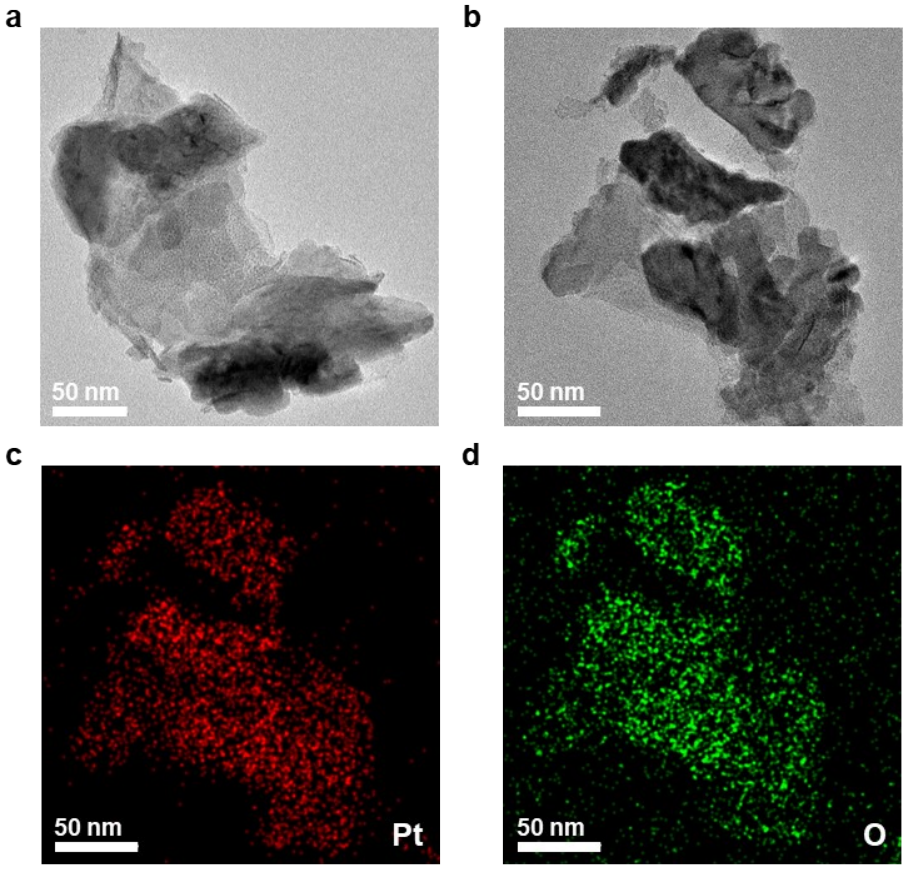

Figure S2. Morphology characterization of α-PtO_2. (**a**, **b**) TEM images of α-PtO_2. The corresponding elemental mappings showing (**c**) Pt (red) and (**d**) O (green) distributions.

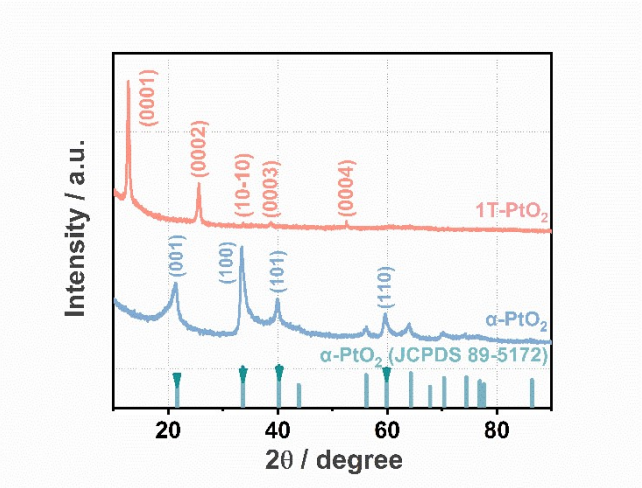

Figure S3. Comparison of XRD patterns of 1T-PtO_2 (orange curve) and α-PtO_2 (blue curve). Sharp Bragg diffraction peaks identify the high crystallinity of 1T-PtO_2 and no diffraction peaks of raw material or α-PtO_2 (JCPDS No. 89-5172) are detected in the XRD pattern of 1T-PtO_2.

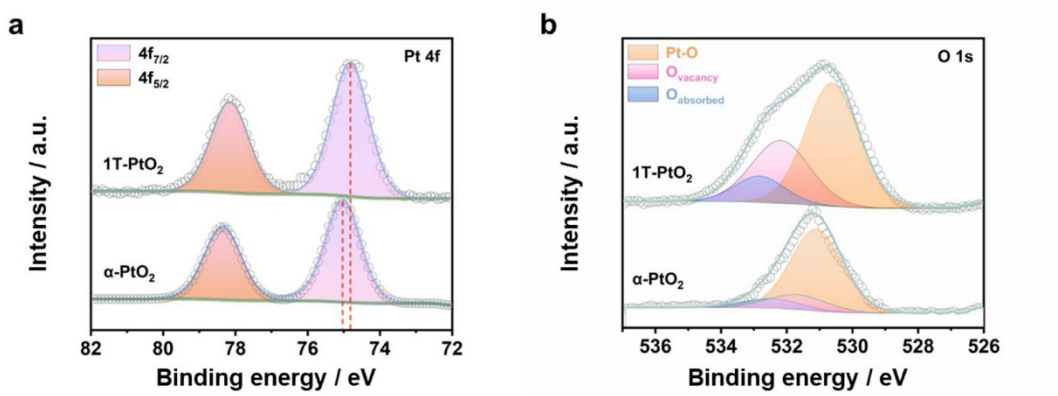

Figure S4. X-ray photoelectron spectroscopy (XPS) spectra of 1T-PtO_2 and α-PtO_2. (**a**) Pt 4f of 1T-PtO_2 and α-PtO_2. (**b**) O 1s of 1T-PtO_2 and α-PtO_2. The O 1s peaks were deconvoluted into three nearly Gaussian components, including the Pt-O lattice bond, oxygen vacancy and surface chemisorbed or dissociated oxygen or OH species, respectively, by fitting analysis.

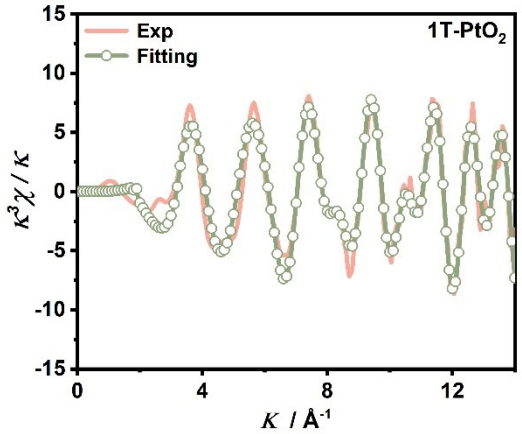

Figure S5. k^3-weighted spectrum at k space and corresponding fitting curve of 1T-PtO_2.

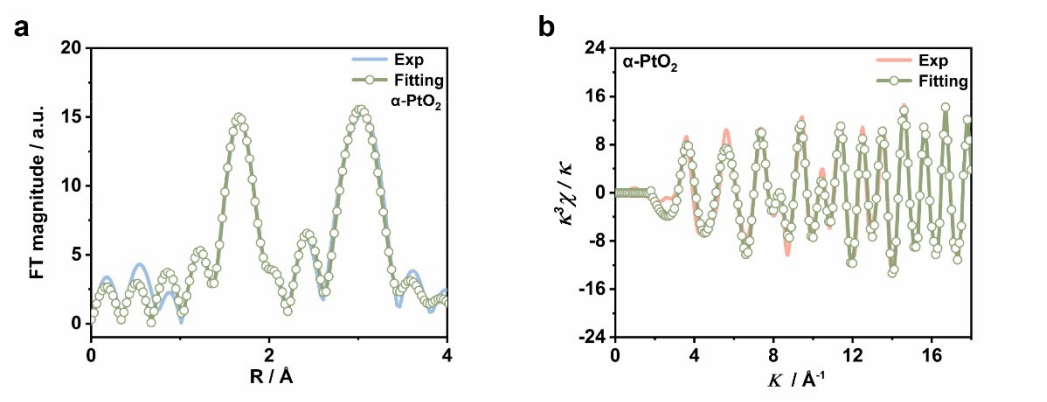

Figure S6. The fitting data of α-PtO_2. (**a**) FT EXAFS spectrum and the corresponding fitting curve of α-PtO_2. (**b**) k^3-weighted spectrum at k space and the corresponding fitting curve of α-PtO_2.

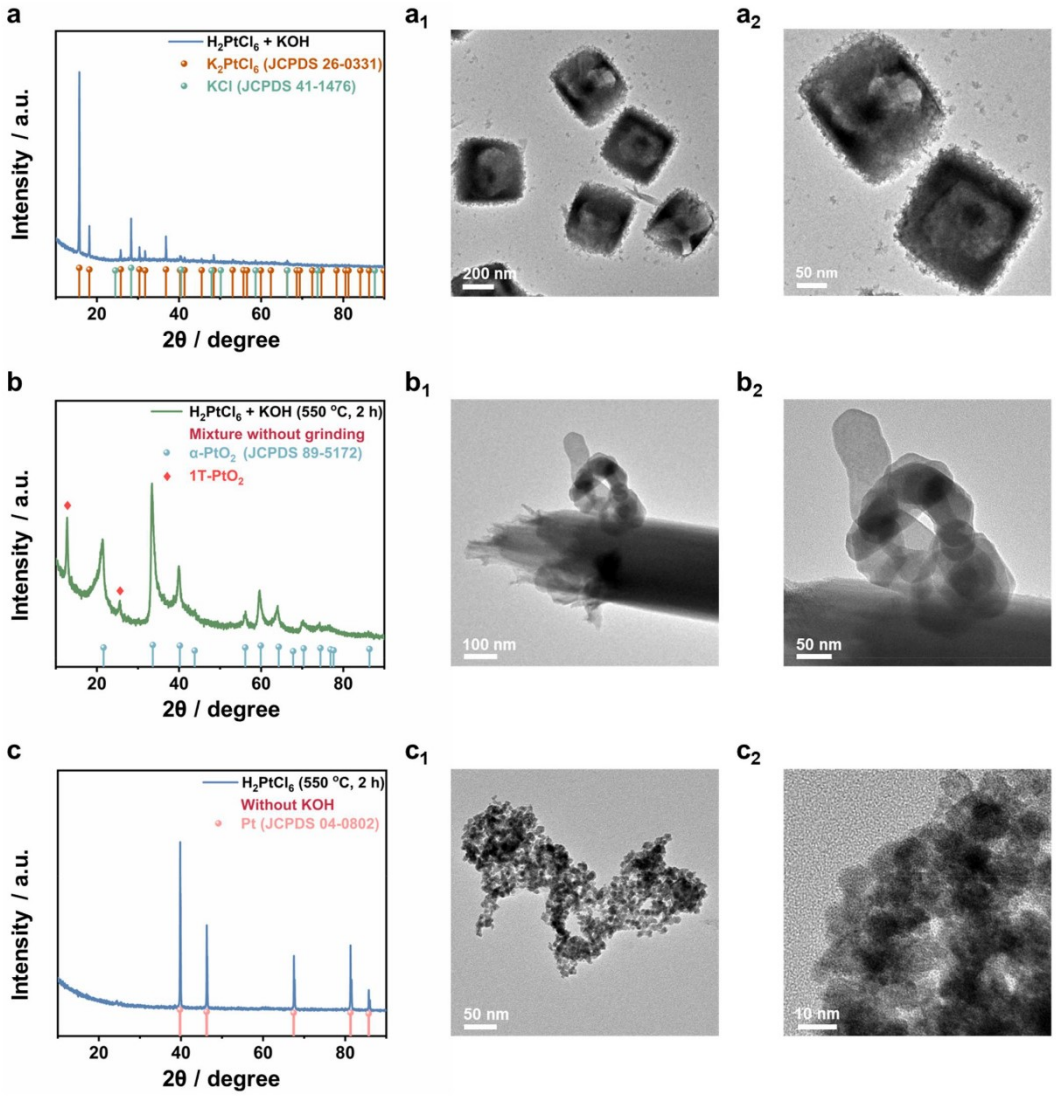

Figure S7. XRD patterns and TEM images of the products obtained by different synthetic conditions. (**a**) The XRD pattern of the product obtained by grinding and mixing H_2PtCl_6 and KOH without the thermal treatment. (**a_1, a_2**) Corresponding TEM images. (**b**) The XRD pattern of the product obtained by directly heating of H_2PtCl_6 and KOH without mechanical force grinding. (**b_1, b_2**) Corresponding TEM images. (**c**) The XRD pattern of the product obtained by mechanical grinding heating without adding KOH. (**c_1, c_2**) Corresponding TEM images.

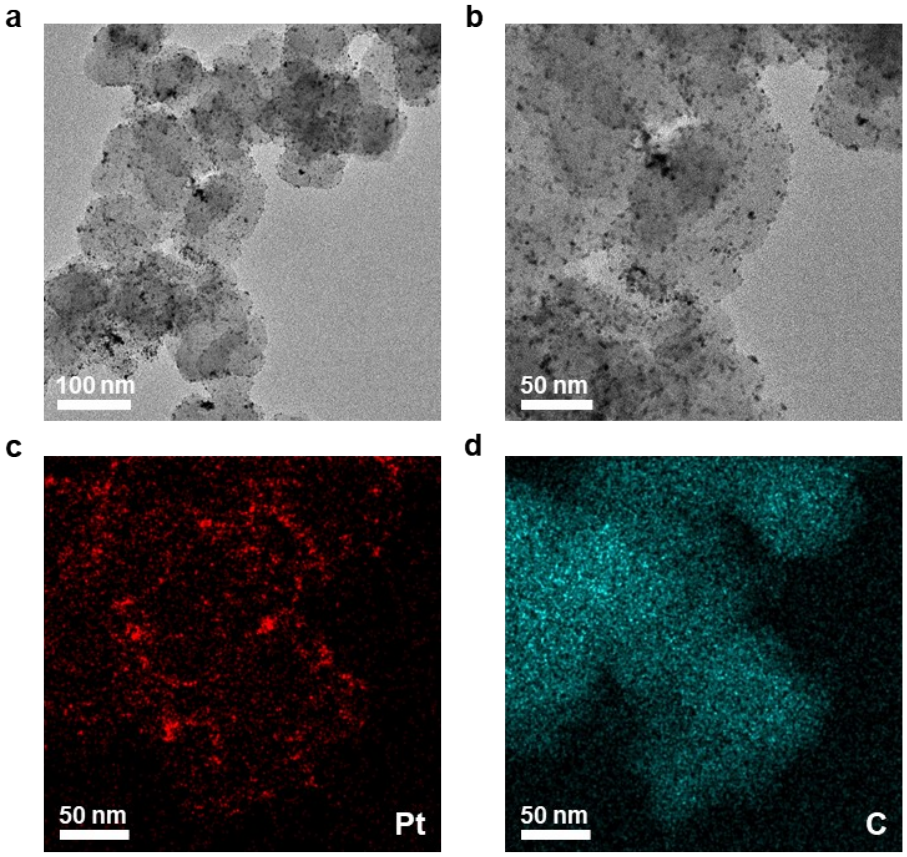

Figure S8. Morphology characterization of 20% Pt/C. (**a**, **b**) TEM images of 20% Pt/C. The corresponding elemental mappings showing (**c**) Pt (red) and (**d**) C (blue) distributions.

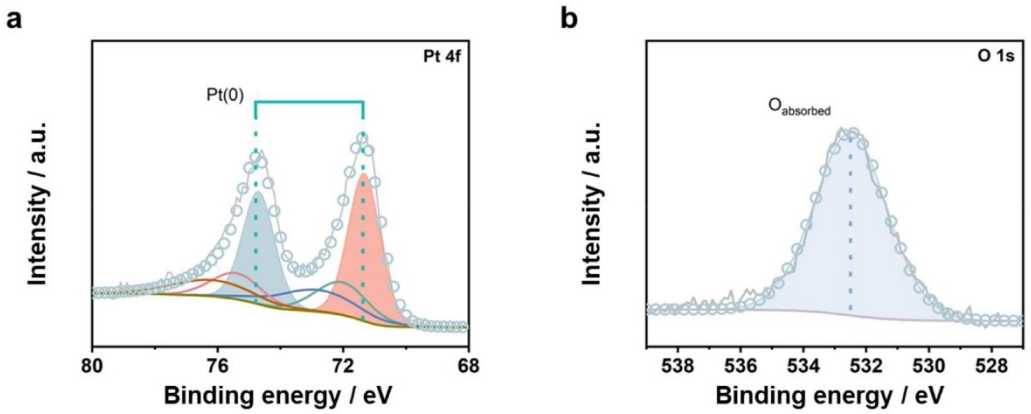

Figure S9. XPS spectra of 20% Pt/C. (**a**) Pt 4f of 20% Pt/C. (**b**) O 1s of 20% Pt/C. The O 1s peaks were deconvoluted into surface chemisorbed or dissociated oxygen or OH species, by fitting analysis.

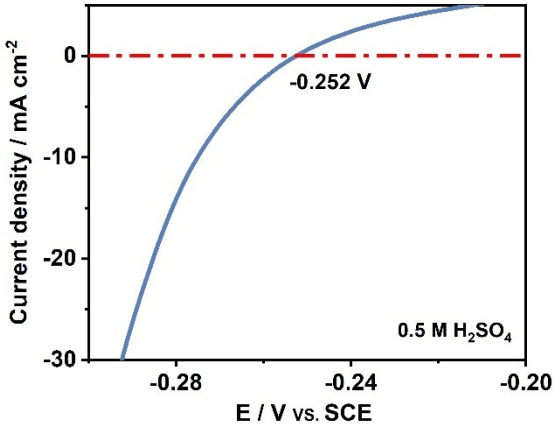

Figure S10. Calibration of the reference electrode. Calibration of the saturated calomel electrode (SCE) electrode with respect to reversible hydrogen electrode (RHE) in 0.5 M H_2SO_4 electrolytes bubbled with pure hydrogen gas at room temperature. Scan rate: 1 mV s^{-1}.

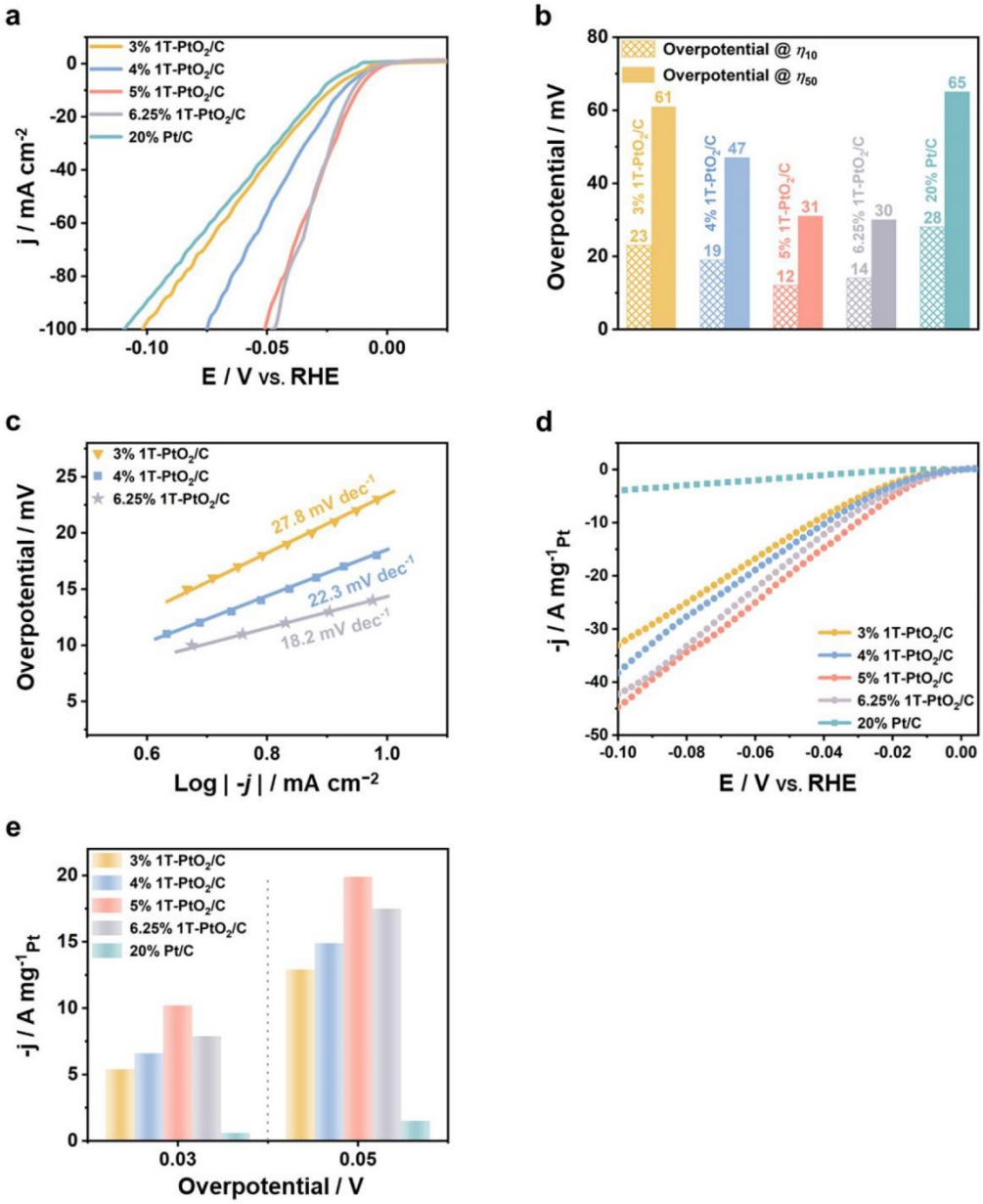

Figure S11. HER performance of different samples. (**a**) LSV curves of catalysts with different 1T-PtO_2 contents and 20% Pt/C in M H_2SO_4. (**b**) Overpotentials of different samples at the current densities of -10 mA cm^{-2} and -50 mA cm^{-2}. (**c**) Tafel slopes of 3% 1T-PtO_2/C, 4% 1T-PtO_2/C and 6.25% 1T-PtO_2/C. (**d**) The polarization curves normalized to the mass loading of different samples. (**e**) Mass activity of catalysts with different 1T-PtO_2 contents and 20% Pt/C at the overpotentials of 30 mV (left) and 50 mV (right).

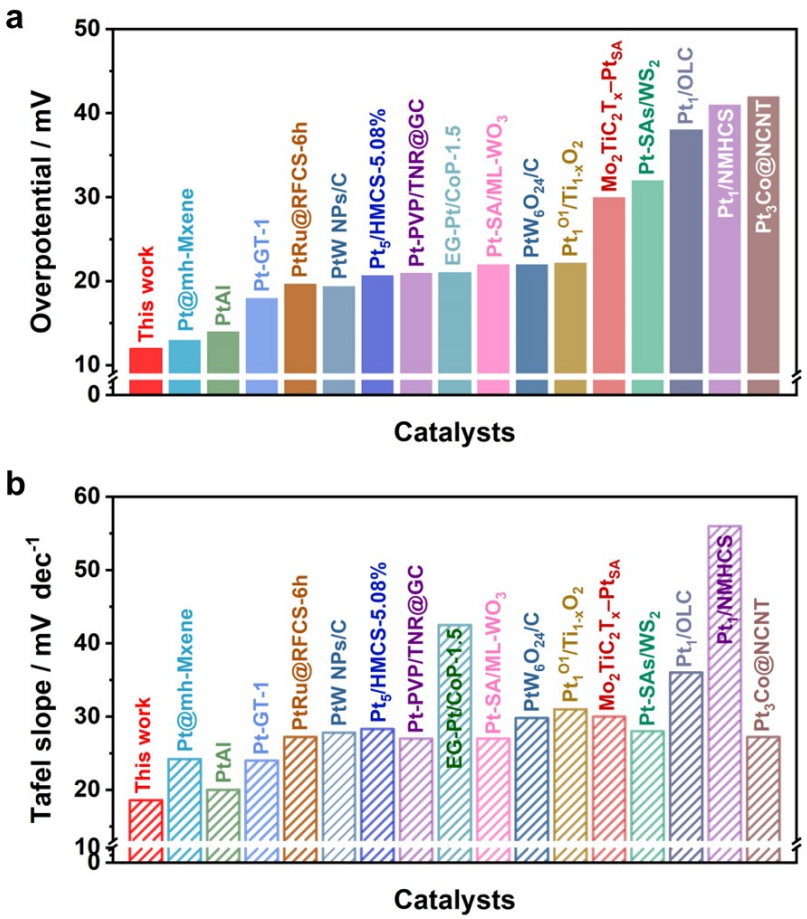

Figure S12. Performance comparison. Comparison of (**a**) the overpotentials at -10 mA cm^{-2} and (**b**) Tafel slopes of this work and available reported catalysts in 0.5 M H_2SO_4, respectively (**Table S5**).

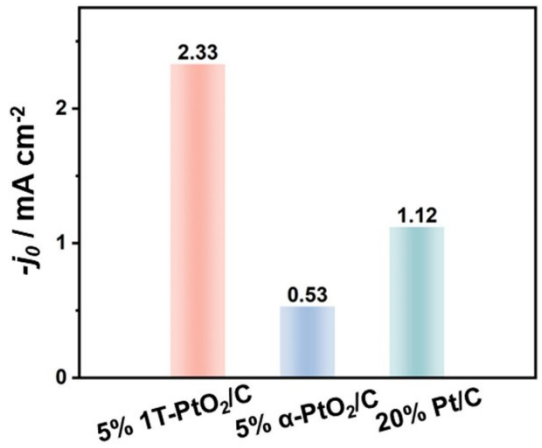

Figure S13. The exchange current density of 5% 1T-PtO_2/C, 5% α-PtO_2/C and 20% Pt/C.

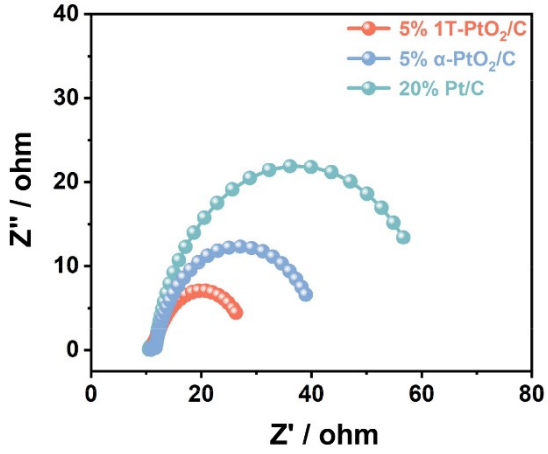

Figure S14. EIS curves of relevant samples for HER in 0.5 M H_2SO_4. The comparison of EIS curves between 5% 1T-PtO_2/C, 5% α-PtO_2/C and 20% Pt/C, and the charge transfer resistance of 5% 1T-PtO_2/C (R_{ct} = 16.79 Ω) is significantly lower than those of 5% α-PtO_2/C (R_{ct} = 30.52 Ω) and 20% Pt/C (R_{ct} = 51.53 Ω).

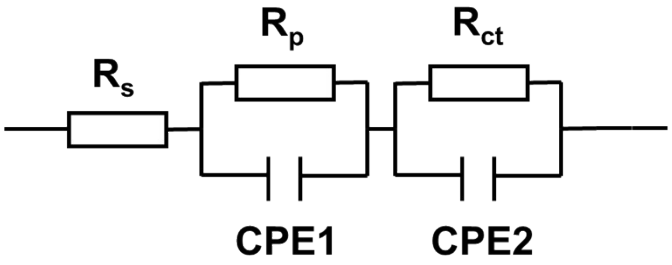

Figure S15. The equivalent circuit. Two-time-constant model equivalent circuit used for data fitting of EIS spectra (R_s is the solution resistance, R_p||CPE1 is associated with the electrode porosity at high-frequency, and R_{ct}||CPE2 is associated with HER kinetics at low-frequency).

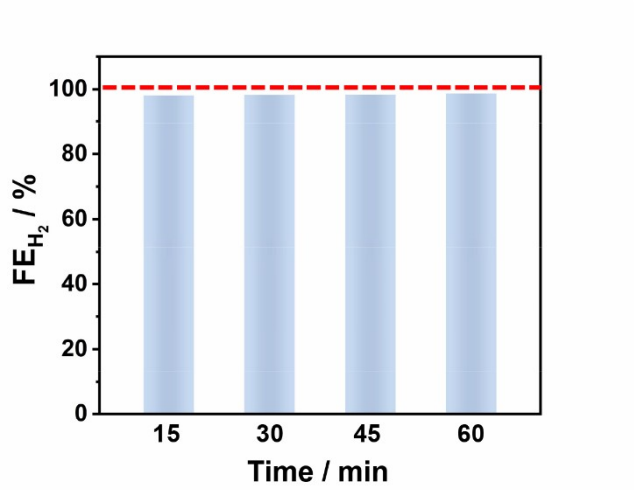

Figure S16. Faradaic efficiency (FE) of HER for 5% 1T-PtO_2/C. FE of HER for 5% 1T-PtO_2/C determined by a gas chromatograph (GC Agilent 7890B). 5% 1T-PtO_2/C was tested at the current density of -10 mA cm^{-2} for 1 h, and the data were collected at an interval of 15 min.

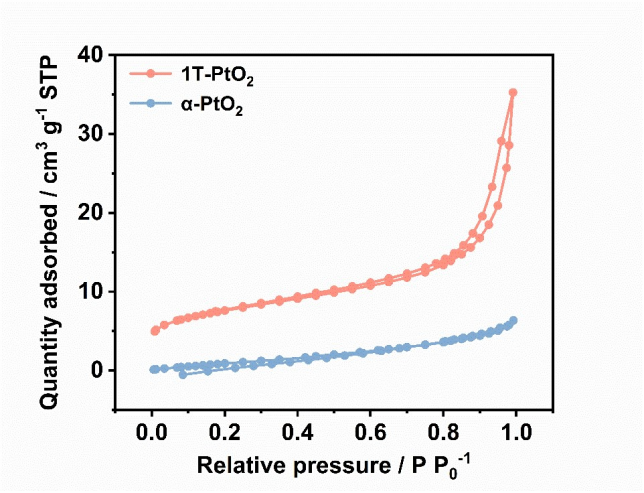

Figure S17. BET surface area measurements. N_2 adsorption-desorption isotherms of 1T-PtO_2 and α-PtO_2.

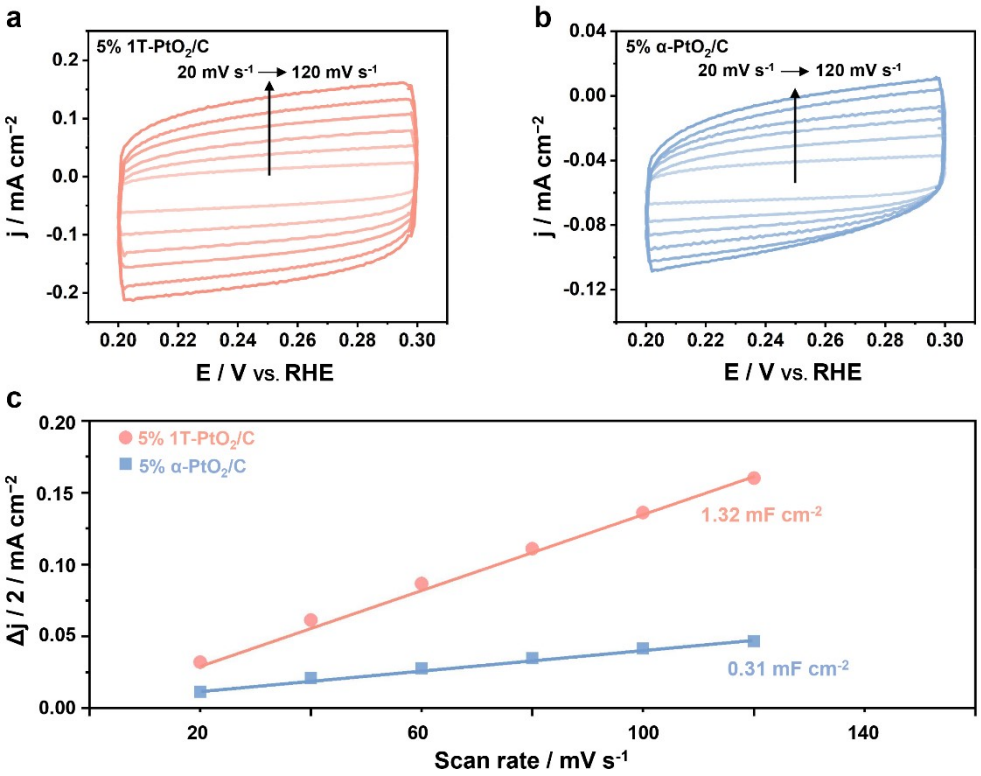

Figure S18. The ECSAs of 5% 1T-PtO_2/C and 5% α-PtO_2/C. (**a**) Cyclic voltammogram curves of 5% 1T-PtO_2/C in a potential region of 0.2 ~ 0.3 V vs. RHE. (**b**) Cyclic voltammogram curves of 5% α-PtO_2/C in a potential region of 0.2 ~ 0.3 V vs. RHE. (**c**) The corresponding plots of the charging current density against scan rates of 5% 1T-PtO_2/C and 5% α-PtO_2/C.

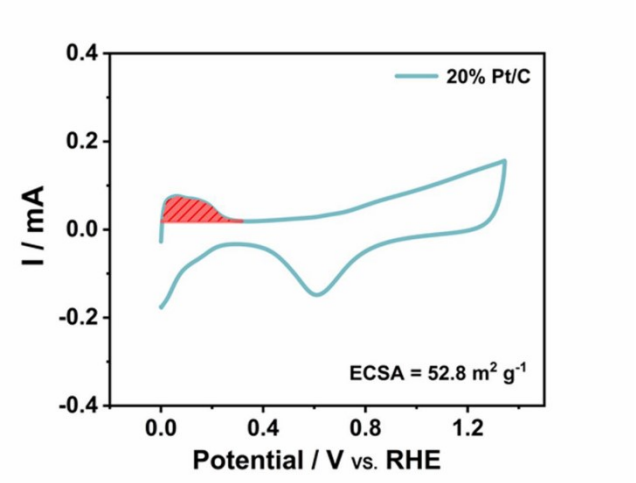

Figure S19. The ECSA of 20% Pt/C. The CV curve of 20% Pt/C in 0.5 M H_2SO_4 with the scan rate of 50 mV s^{-1}.

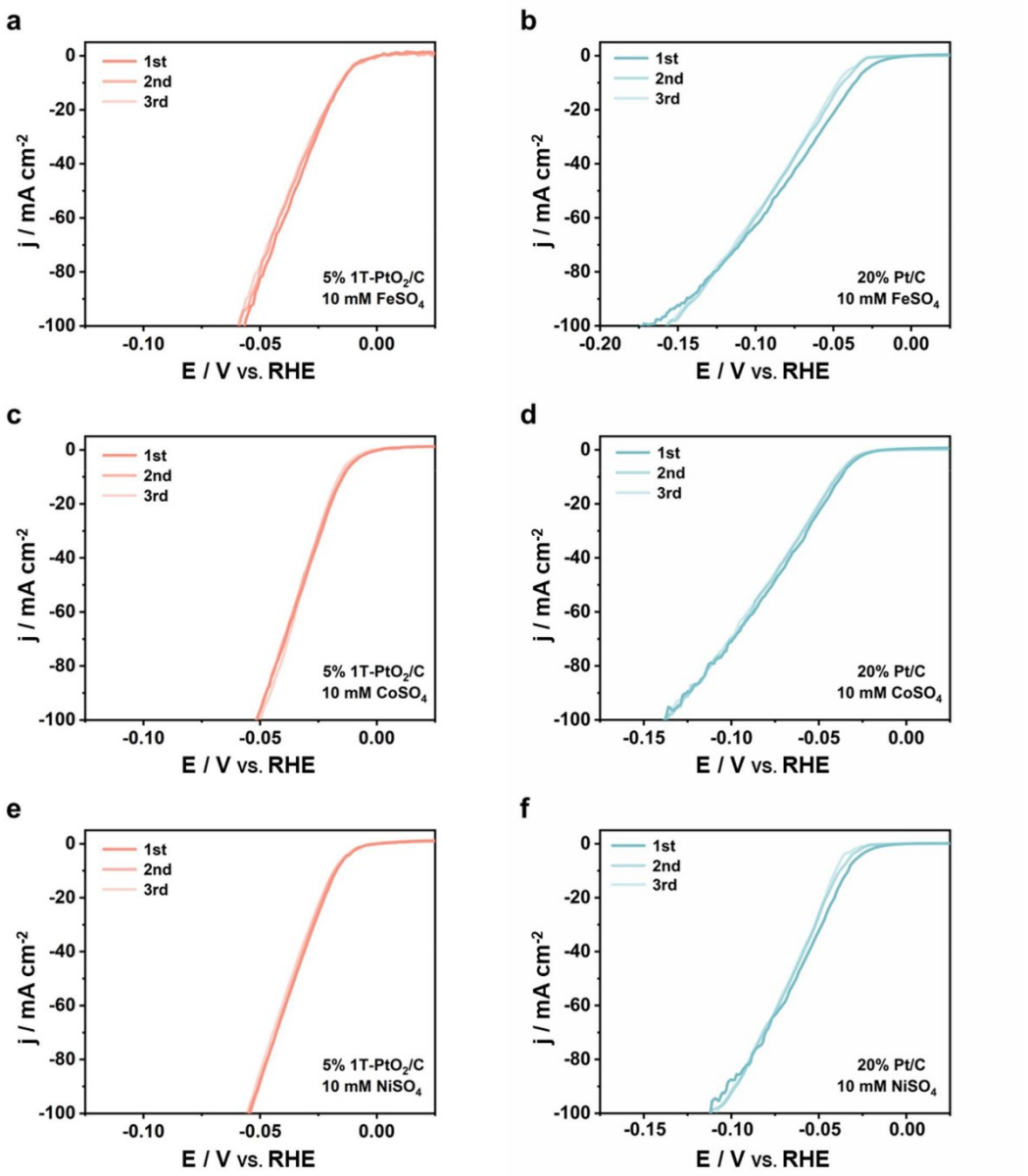

Figure S20. Anti-toxicity test of 5% 1T-PtO_2/C and 20% Pt/C. The HER polarization curves of 5% 1T-PtO_2/C in (**a**) 0.5 M H_2SO_4 + 10 mM $FeSO_4$, (**c**) 0.5 M H_2SO_4 + 10 mM $CoSO_4$ and (**e**) 0.5 M H_2SO_4 + 10 mM $NiSO_4$, respectively. The HER polarization curves of 20% Pt/C in (**b**) 0.5 M H_2SO_4 + 10 mM $FeSO_4$, (**d**) 0.5 M H_2SO_4 + 10 mM $CoSO_4$ and (**f**) 0.5 M H_2SO_4 + 10 mM $NiSO_4$, respectively.

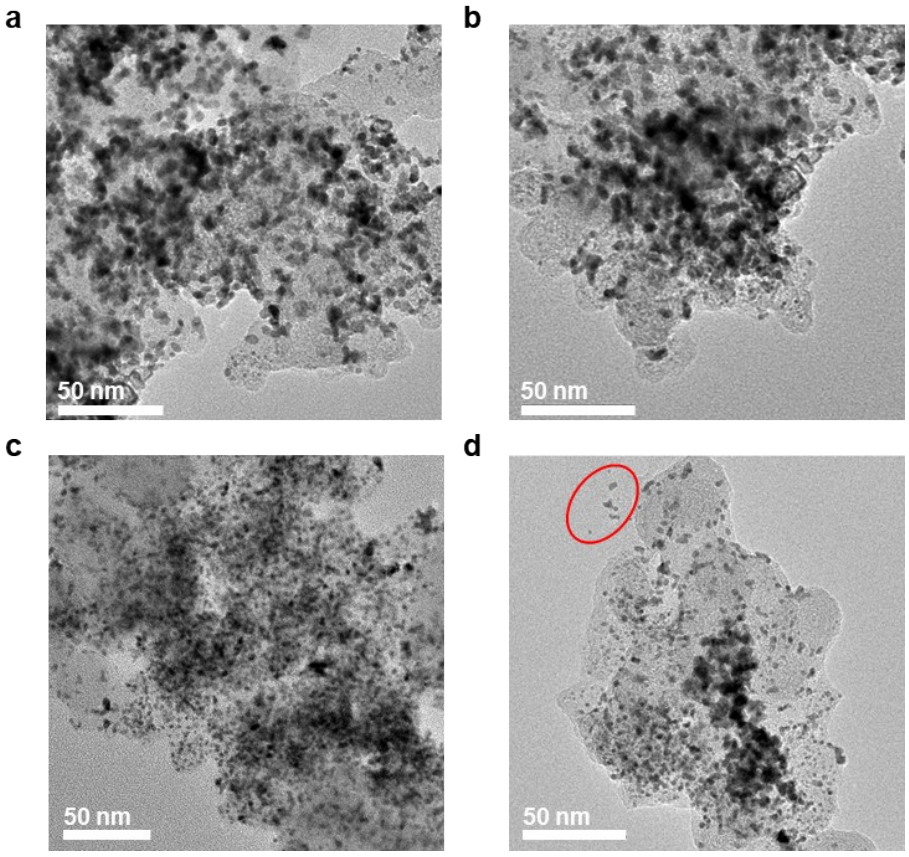

Figure S21. The TEM images of 20% Pt/C after stability test. (**a**)-(**d**) After the stability test, the Pt particles on the carbon carrier had obvious agglomeration, and the phenomenon of Pt particles falling off from the carbon carrier was observed at the same time, which may be the reason for the poor stability of 20% Pt/C.

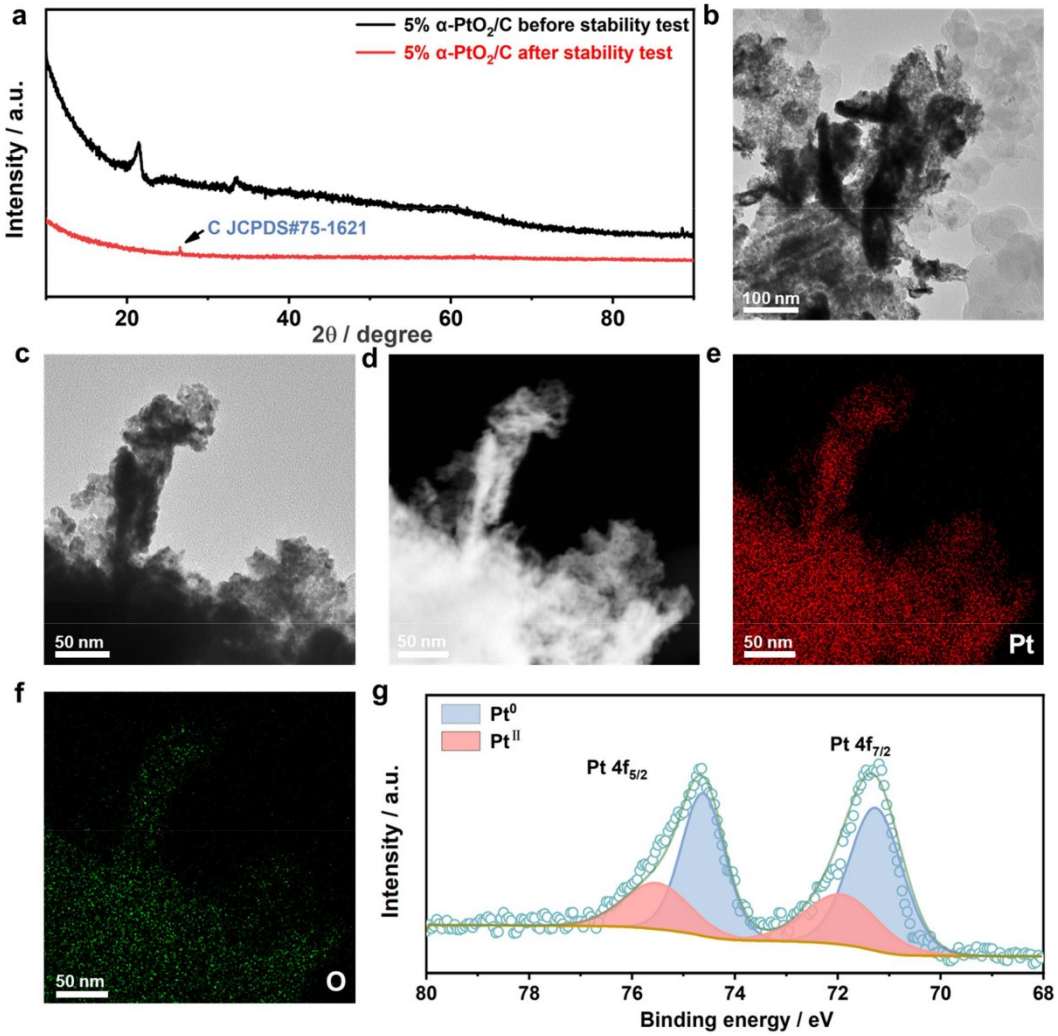

Figure S22. Characterizations of the 5% α-PtO_2/C after the stability test. (**a**) The XRD patterns comparison 5% α-PtO_2/C before and after stability test in 0.5 M H_2SO_4. The XRD diffraction peak at 26.3° corresponds to the (002) peak of C (JCPDS#75-1621). (**b**) and (**c**) The TEM images of 5% α-PtO_2/C after stability test. (**d**)-(**f**) TEM-EDX mapping of 5% α-PtO_2/C after stability test. (**g**) Pt 4f peak of α-PtO_2 after stability test. After the stability test, the valence of platinum changed significantly.

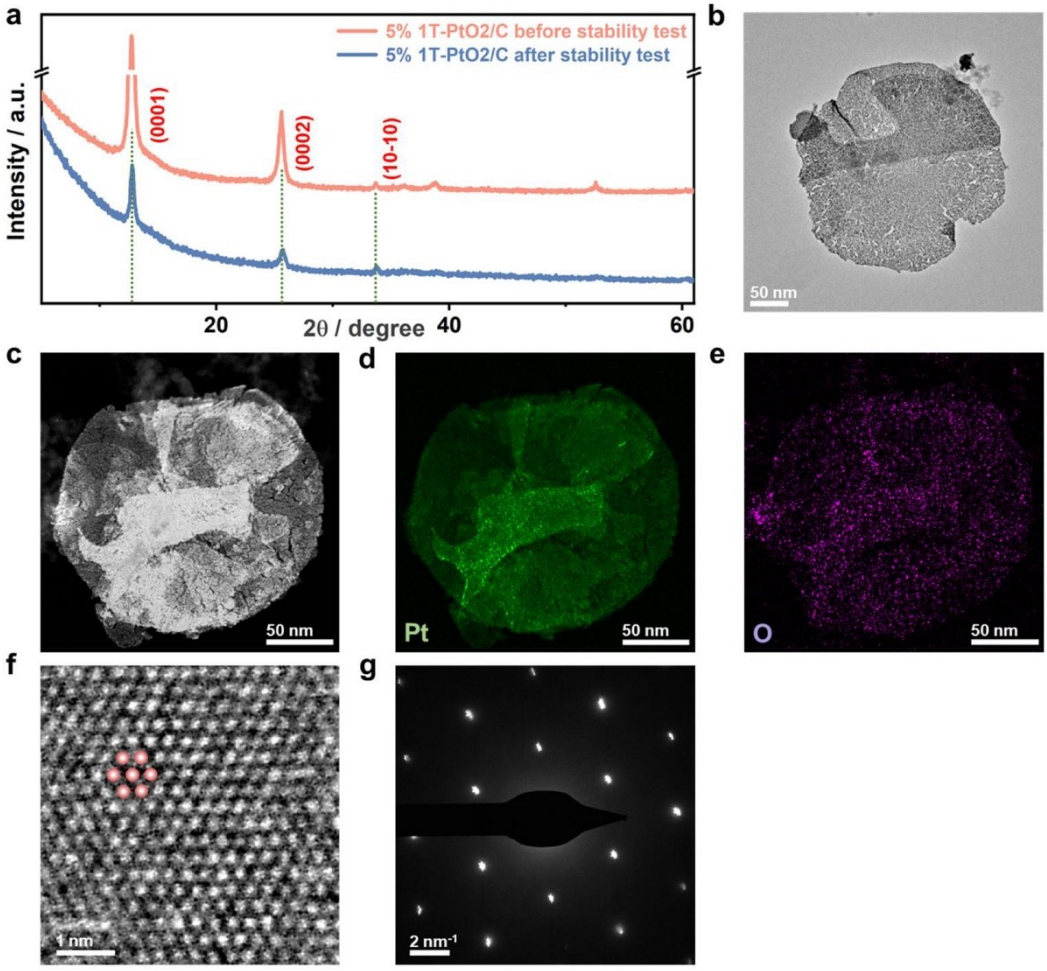

Figure S23. Characterizations of the 5% 1T-PtO_2/C after the stability test. (**a**) The XRD patterns comparison 5% 1T-PtO_2/C before and after stability test in 0.5 M H_2SO_4. (**b**) The TEM image of 5% 1T-PtO_2/C after stability test. (**c**)-(**e**) TEM-EDX mapping of 5% 1T-PtO_2/C after stability test, where Pt and O are uniformly distributed. (**f**) The STEM-ADF image of 1T-PtO_2 after the stability test, showing the hexagonal pattern of Pt elements. (**g**) The ED pattern of 1T-PtO_2 after the stability test, showing the hexagonal arrangement.

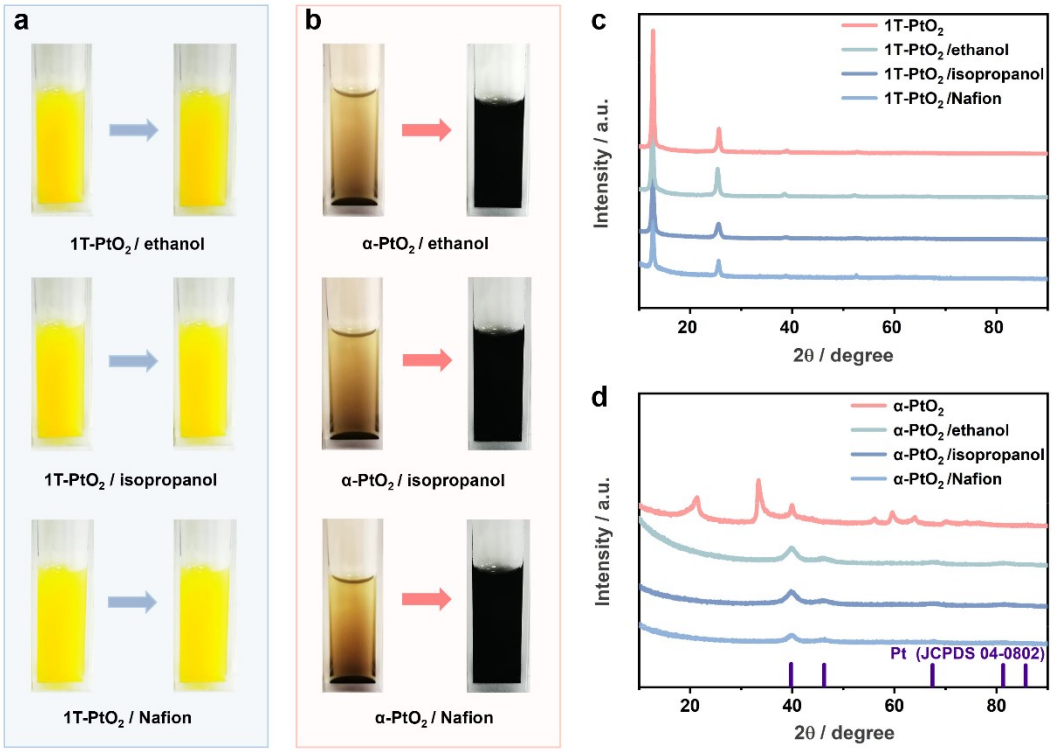

Figure 24. Chemical stability of 1T-PtO_2 and α-PtO_2 in ethanol, isopropanol and Nafion solution. (**a**) Comparison before (left) and after (right) continuous ultrasonic dispersion of 1T-PtO_2 in the corresponding solution for 5 hours and (**c**) the corresponding XRD patterns. (**b**) Comparison before (left) and after (right) continuous ultrasonic dispersion of α-PtO_2 in the corresponding solution for 1 hour and (**d**) the corresponding XRD patterns.

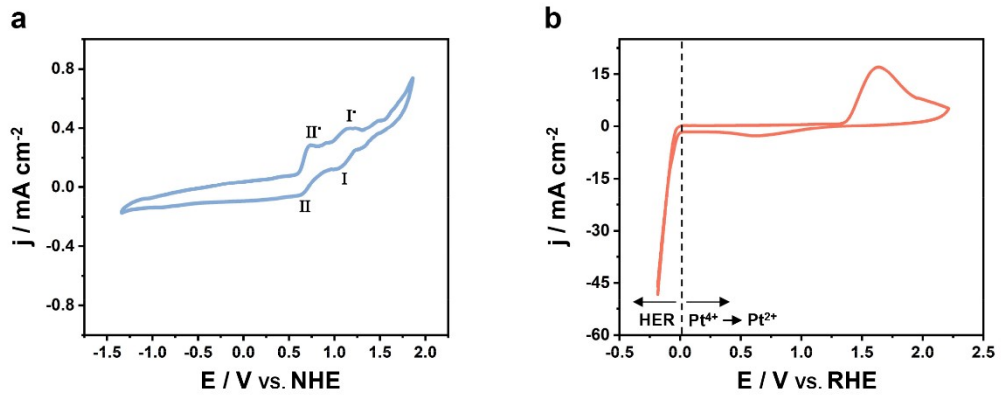

Figure S25. The CV of 1T-PtO_2 in acetonitrile and 0.5 M H_2SO_4. (**a**) CV of 1T-PtO_2 in acetonitrile with the scan rate of 20 mV s^{-1}. The two redox peaks for I and II are attributed to Pt (IV) → Pt (III) and Pt (III) → Pt (II) processes, respectively. NHE: Normal hydrogen electrode. (**b**) CV of 1T-PtO_2 in 0.5 M H_2SO_4 with the scan rate of 20 mV s^{-1}.

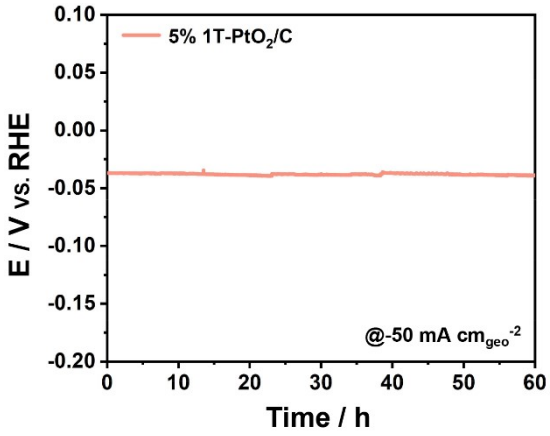

Figure S26. V-t curves of 5% 1T-PtO_2/C at the constant current density of 50 mA cm^{-2}.

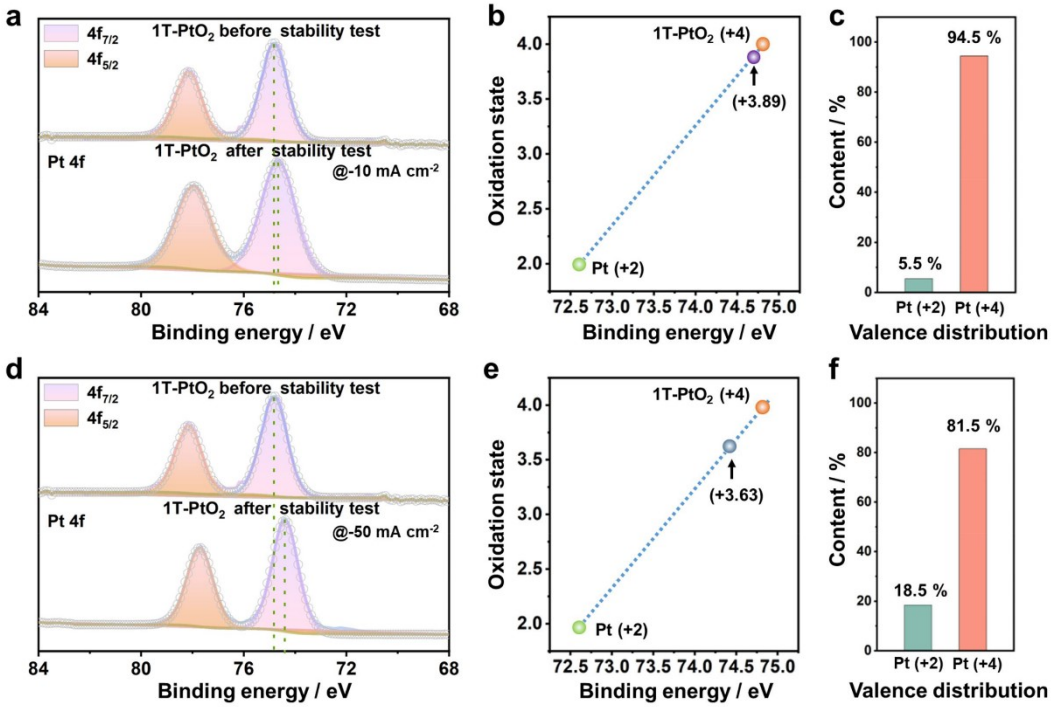

Figure S27. Valence state analysis of Pt. (**a**) Pt 4f peak of 1T-PtO_2 before and after stability test at the constant current density of 10 mA cm^{-2}. (**b**) According to Pt 4f peak of the $Pt(OH)_2$, 1T-PtO_2 before and after stability test at the constant current density of 10 mA cm^{-2}, the fitted curve correlating with the average oxidation state of Pt was obtained. (**c**) Pt (+3.89) valence distribution. (**d**) Pt 4f peak of 1T-PtO_2 before and after stability test at the constant current density of 50 mA cm^{-2}. (**e**) According to Pt 4f peak of the $Pt(OH)_2$, 1T-PtO_2 before and after stability test at the constant current density of 50 mA cm^{-2}, the fitted curve correlating with the average oxidation state of Pt was obtained. (**f**) Pt (+3.63) valence distribution.

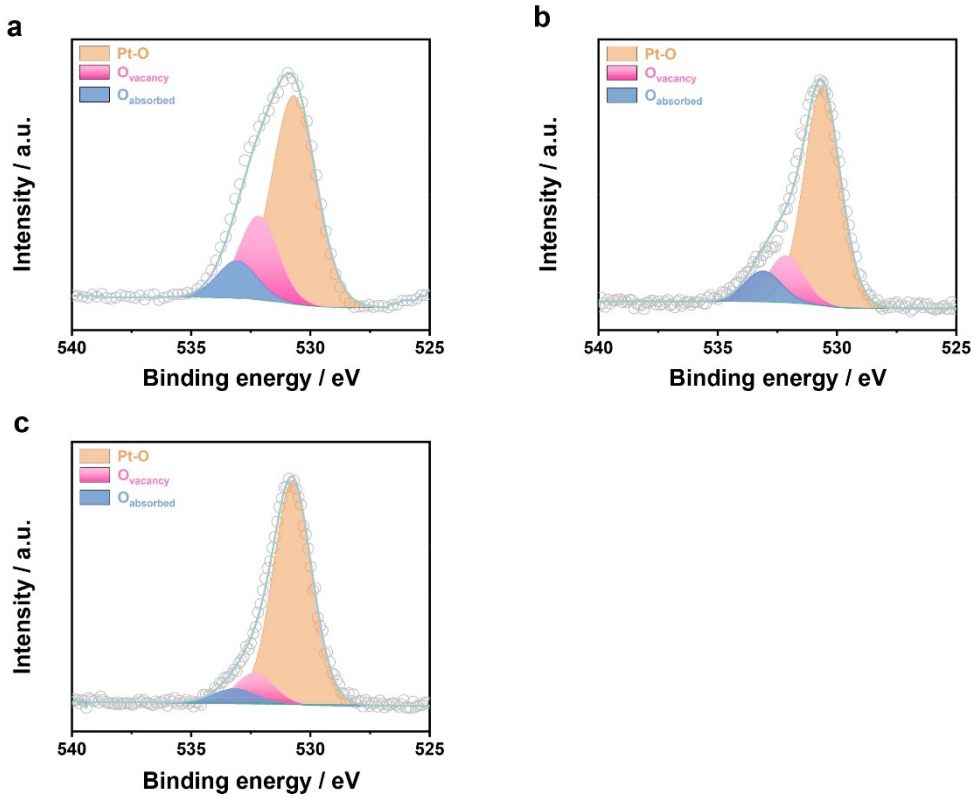

Figure S28. O 1s XPS of 1T-PtO_2 before and after stability test. (**a**) O 1s peak of 1T-PtO_2 before stability test. (**b**) O 1s peak of 1T-PtO_2 after stability test at the constant current density of 10 mA cm^{-2}. (**c**) O 1s peak of 1T-PtO_2 after stability test at the constant current density of 50 mA cm^{-2}.

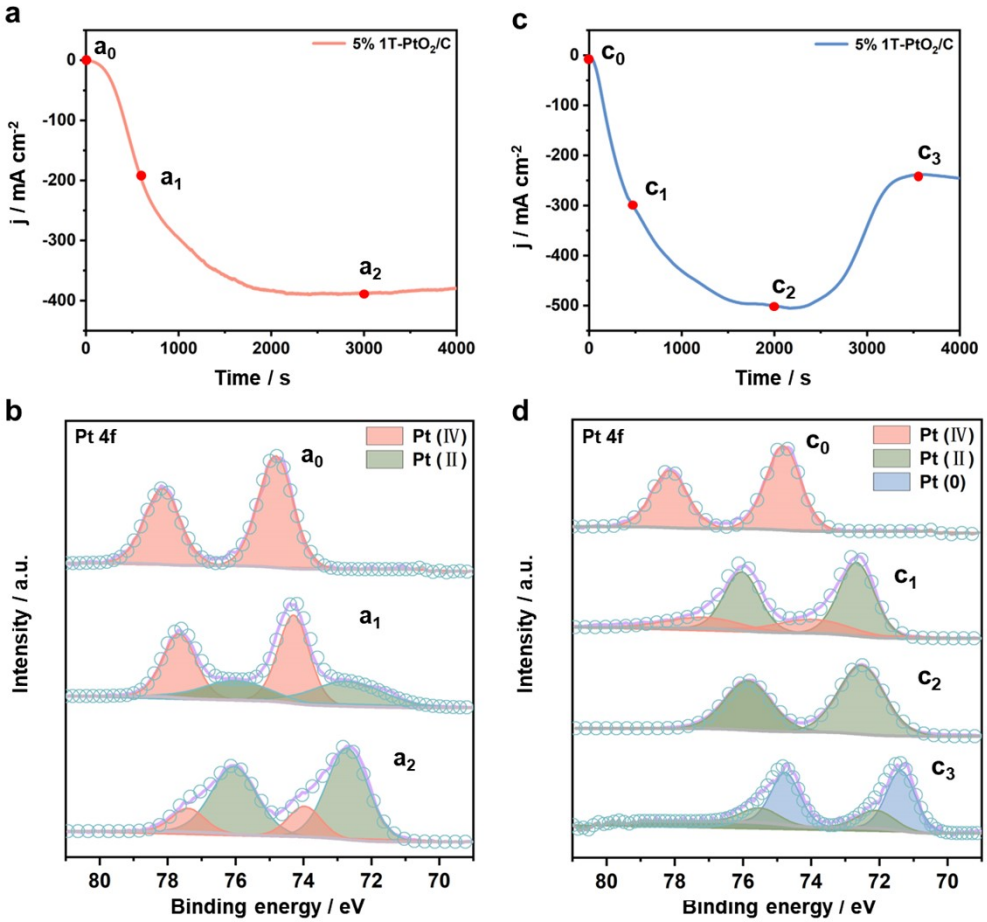

Figure S29. Valence state analysis of Pt. (**a**) I-t curves of 5% 1T-PtO_2/C at the voltage of -0.4 V in 0.5 M H_2SO_4. (**b**) Pt 4f peak of different locations in the HER reaction process. (**c**) I-t curves of 5% 1T-PtO_2/C at the voltage of -0.5 V in 0.5 M H_2SO_4. (**d**) Pt 4f peak of different locations in the HER reaction process.

Supporting Figures

Table S1. Crystal structure parameters for the EXAFS fitting using the ARTEMIS module.

Sample	Shell	CN	R / Å	σ^2 / 10^{-3} Å^2	ΔE_0 / eV	R-factor
1T-PtO_2	Pt-O	6	2.0239	0.0024 ± 0.0006	14.1054 ± 2.0381	0.008
	Pt-Pt	6	3.0863	0.0031 ± 0.0007	11.8438 ± 2.2863	0.008
α-PtO_2	Pt-O	6	2.0267	0.0034 ± 0.0007	12.3241 ± 2.1613	0.006
	Pt-Pt	6	3.1074	0.0033 ± 0.0005	12.6056 ± 1.6245	0.006

CN: coordination number; R: bond length; σ^2: Debye-Waller factors; ΔE_0: inner potential shift and R-factor: goodness of fit.

Table S2. The dosage of corresponding substances of different catalysts, then the Pt loading of composite catalyst was accurately measured by ICP.

Catalyst	Dosage of 1T-PtO_2 / mg	Dosage of carbon powder / mg	Mass content of 1T-PtO_2 / %	Mass content of Pt / % (ICP)
3% 1T-PtO_2/C	1	32	3.03	2.58
4% 1T-PtO_2/C	1	24	4.00	3.42
5% 1T-PtO_2/C	1	19	5.00	4.27
6.25% 1T-PtO_2/C	1	15	6.25	5.38
5% α-PtO_2/C	1	19	5.00	4.26

Table S3. The overpotentials of several catalysts at different current densities.

Catalyst	3% 1T-PtO_2/C	4% 1T-PtO_2/C	5% 1T-PtO_2/C	6.25% 1T-PtO_2/C	20% Pt/C
η_{10} / mV	23	19	12	14	28
η_{50} / mV	61	47	31	30	65
η_{100} / mV	102	75	51	49	110

Table S4. Mass activities of different catalysts at the overpotentials of 30 mV and 50 mV (j / A·mg^{-1}_{Pt}).

Catalyst	3% 1T-PtO_2/C	4% 1T-PtO_2/C	5% 1T-PtO_2/C	6.25% 1T-PtO_2/C	20% Pt/C
$j@\eta_{30}$ / A mg^{-1}_{Pt}	-5.4	-6.6	-10.2	-7.9	-0.5
$j@\eta_{50}$ / A mg^{-1}_{Pt}	-12.9	-14.9	-19.9	-17.5	-1.5

Table S5. The comparison of HER activity performances of 5% 1T-PtO_2/C and the reported electrocatalysts.

Catalyst	Substrate	Electrol-yte	Catalyst loading / mg cm^{-2}	Overpotential @ -10 mA cm_{geo}^{-2} / mV	Tafel slope / mV dec^{-1}	Refs
5% 1T-PtO_2/C	**GCE**	**0.5 M H_2SO_4**	**0.14**	**12**	**18.6**	**This work**
Pt_1/OLC	RDE	0.5 M H_2SO_4	0.51	38	36	*Nat. Energy* **2019**, *4,* 512-518
Pt-GT-1	graphite paper	0.1 M $HClO_4$	0.28	18	24	*Nat. Energy* **2018**, *3*, 773-782
Mo_2TiC_2Tx–Pt_{SA}	carbon paper	0.05 M H_2SO_4	1	30	30	*Nat. Catal.* **2018**, *1*, 985-992
Pt-SAs /WS_2	GCE	0.5 M H_2SO_4	0.01	32	28	*Nat.Commun.* **2021**, *12*, 3021
PtW_6O_{24}/C	GCE	0.5 M H_2SO_4	-	22	29.8	*Nat. Commun.* **2020**, *11*, 490
Pt_1/N-C	GCE	0.5 M H_2SO_4	0.25	19	14.2	*Nat. Commun.* **2020**, *11*, 1029
Pt–Ru	RDE	0.5 M H_2SO_4	0.15	-	28.9	*Nat. Commun.* **2019**, *10*, 4936
PtNC/S–C	RDE	0.5 M H_2SO_4	-	11	23.5	*Nat. Commun.* **2019**, *10*, 4977
ALDPt/NGN	RDE	0.5 M H_2SO_4	0.05	-	29	*Nat. Commun.* **2019**, *7*, 13638
PtW NPs /C	RDE	0.5 M H_2SO_4	0.127	19.4	27.8	*J. Am. Chem. Soc.* **2020**, *142*, 17250-17254
Pt_1/NMHCS	GCE	0.5 M H_2SO_4	0.412	41	56	*Adv. Mater.* **2021**, *33*, 2008599
PtGa	Ti wire	0.5 M H_2SO_4	-	13.3	16	*Adv. Mater.* **2021**, *32*, 1908518
PtAl	Ti wire	0.5 M H_2SO_4	-	14	20	*Adv. Mater.* **2021**, *32*, 1908518
Pt_5/HMCS-5.08%	GC	0.5 M H_2SO_4	0.16	20.7	28.3	*Adv. Mater.* **2020**, *32*, 1901349

Pt_3Co@NCNT	CFP	0.5 M H_2SO_4	0.38	42	27.2	*Angew. Chem. Int. Ed.* **2021**, *60*, 19068-19073
Pt_1^{O1}/ $Ti_{1-x}O_2$	GCE	0.5 M H_2SO_4	0.3	22.2	31	*Angew. Chem. Int. Ed.* **2020**, *59*, 17712-17718
Pt-PVP/ TNR@GC	RDE	0.5 M H_2SO_4	1.25	21	27	*Angew. Chem. Int. Ed.* **2020**, *59*, 15902-15907
Pt-SA /ML-WO_3	GC	0.5 M H_2SO_4	0.56	22	27	*Adv. Funct. Mater.* **2021**, *31*, 2009770
EG-Pt/ CoP-1.5	CFP	0.5 M H_2SO_4	0.102	21	42.5	*Energy Environ. Sci.* **2019**, *12*, 2298-2304
Pt SASs /AG	GCE	0.5 M H_2SO_4	7.07	12	29.33	*Energy Environ. Sci.* **2019**, *12*, 1000-1007
PtRu@RFCS-6h	GCE	0.5 M H_2SO_4	0.354	19.7	27.2	*Energy Environ. Sci.* **2018**, *11*, 1232-1239

Table S6. The element composition of same samples before and after stability test based on Figure S27 and Figure S28.

Sample	Peak	Atom [%]	Atomic ratio
1T-PtO_2	Pt 4f	33.54	O:Pt = 1.98:1
	O 1s	66.46	
1T-PtO_2 after stability test (10 mA cm^{-2})	Pt 4f	34.13	O:Pt = 1.93:1
	O 1s	65.87	
1T-PtO_2 after stability test (50 mA cm^{-2})	Pt 4f	35.59	O:Pt = 1.81:1
	O 1s	64.41	